Measurement of the math xmlns="http://www.w3.org/1998/Math/MathML">mrow>mmultiscripts>mi>Mo/mi>mprescripts>/mprescripts>none>/none>mn>100/mn>/mmultiscripts>mo>(/mo>mi>α/mi>mo>,/mo>mi>x/mi>mi>n/mi>mo>)/mo>/mrow>/math> cross section at weak math xmlns="http://www.w3.org/1998/Math/MathML">mi>r/mi>/math>-process energies

W.-J. Ong, M. L. Avila, P. Mohr, K. E. Rehm, D. Santiago-Gonzalez, J. Chen, C. R. Hoffman, Z. Meisel, F. Montes, and J. Pereira

Phys. Rev. C **105**, 055803 — Published 12 May 2022

DOI: 10.1103/PhysRevC.105.055803

Measurement of the ^{100}Mo(α, xn) cross-section at weak r-process energies

W.-J. Ong,[1,2,3] M.L. Avila,[2] P. Mohr,[4] K.E. Rehm,[2] D. Santiago-Gonzalez,[2]
J. Chen,[2] C.R. Hoffman,[2] Z. Meisel,[5,3] F. Montes,[6,3] and J. Pereira[6,3]

[1] *Nuclear and Chemical Sciences Division, Lawrence Livermore National Laboratory, Livermore, CA 94550, USA*
[2] *Physics Division, Argonne National Laboratory, Lemont, IL 60439, USA*
[3] *Joint Institute for Nuclear Astrophysics - Center for the Evolution of the Elements, Michigan State University, East Lansing, MI 48824, USA*
[4] *Institute for Nuclear Research (MTA Atomki) H-4001 Debrecen, Hungary*
[5] *Department of Physics and Astronomy, Ohio University, Athens, OH 45701, USA*
[6] *National Superconducting Cyclotron Laboratory, Michigan State University, East Lansing, MI 48824, USA*

(Dated: March 31, 2022)

The weak r-process in neutrino-driven winds following a core-collapse supernova is thought to contribute to the cosmic abundances of the first r-process peak elements between Se and Ag. Sensitivity studies have found that the early nucleosynthesis in the weak r-process is primarily driven by (α, xn) reactions due to the high temperatures, and that current nuclear physics uncertainties in the (α, xn) rates result in significant uncertainties of the calculated abundances. The weak r-process path proceeds several nuclei away from stability where (α, xn) reaction cross-sections have not yet been measured. In this work we report the ^{100}Mo(α, xn) cross-section (between 8.9 MeV and 13.2 MeV in the center of mass, corresponding to 3.5-6.8 GK) in inverse kinematics using the Multi-Sampling Ionization Chamber (MUSIC) detector at the Argonne Tandem Linac Accelerator System (ATLAS) facility. With this first measurement of the ^{100}Mo(α, xn) cross-section, we have demonstrated the ability of MUSIC to measure (α, xn) cross-sections for A up to 100, therefore paving the way for further measurements with radioactive beams at ATLAS or the Facility for Rare Isotope Beams (FRIB).

I. INTRODUCTION

The origin(s) of the first peak in the rapid neutron capture process (r-process) has not been unambiguously determined. While some of the galactic abundance is likely to have been produced by neutron star mergers, as evidenced by the direct observation of Sr spectral lines [1] in the electromagnetic radiation from the neutron star merger GW170817, this does not preclude the possibility of at least one other astrophysical production site. Observations of metal-poor stars show that their first r-process peak abundances show remarkable variations, unlike the second and third peaks which show robustness amongst disparate stars [2]. This suggests that while the second and third peaks likely have a single astrophysical site, the synthesis of the first peak probably sees contributions from several sources.

The neutrino-driven wind following a core-collapse supernova has been proposed as a potential candidate for producing first r-process peak elements (e.g. [3–5]). In this scenario, the large neutrino flux from the newly formed proto-neutron star converts free protons into neutrons, allowing for a momentary burst of high neutron flux that leads to r-process nucleosynthesis. However, the neutron-to-seed ratio in this scenario is not high enough for the full r-process to proceed and halts at elements around Z$\sim$47, depending on conditions, and neutrino-driven winds are not expected under realistic conditions to produce the second and third r-process peaks [6]. This scenario is frequently termed the 'weak r-process' to distinguish it from the robust full r-process that occurs in neutron star mergers [7].

The exact elemental abundances produced by the weak r-process are not well-determined. Aside from uncertainty in the physical conditions, such as the entropy or the neutrino spectrum, nuclear physics uncertainties contribute significantly to the total uncertainty in the abundances of the synthesized material. A recent sensitivity study [8, 9] showed that the inclusive (α, xn) reactions dominate the early reaction flow in the neutrino-driven wind. This is because the temperatures are high enough that the neutron-rich material is in (n, γ)-(γ, n) equilibrium and β decays are too slow relative to the timescale (10s of seconds) of the winds. While the wind is in (n, γ)-(γ, n) equilibrium, the relative abundances along a given isotopic chain are determined only by the difference in masses, hence the inclusive (α, xn) rate is needed to determine the reaction flow that increases the proton number. The lack of experimental (α, xn) reaction rate data means that nucleosynthesis calculations rely primarily on Hauser-Feshbach rate estimates. The same sensitivity study demonstrated the need for experimental measurements, showing that realistic variations in the physics input parameters in the Hauser-Feshbach code TALYS could produce up to factors of 100 variations in the calculated (α, xn) reaction rates.

Radioactive beam facilities now produce beams of the nuclei participating in weak r-process reaction flow at high enough intensities for direct measurements of cross-sections to be made on radioactive, neutron-rich nuclei. The Multi-Sampling Ionization Chamber (MUSIC) [10] is a high-efficiency, self-normalizing detector which is well-suited for measuring (α, xn) cross-sections in inverse kinematics. It has been demonstrated to be able to reli-

ably measure (α, n) and (α, p) reaction rates with beams of A<40 [11, 12]. In this work, we show that this technique can be applied for incident beams of A∼100 nuclei, allowing the direct measurement of important (α, xn) reactions in the weak r-process. As MUSIC-type detectors measure the inclusive (α, xn) cross-section, the astrophysically relevant $Z \rightarrow Z+2$ rate can be derived from the experimental data, independent of the dominance of the $(\alpha, 1n)$ or $(\alpha, 2n)$ channels. To ensure clarity in this work, we will refer to the separate (α, xn) channels by $(\alpha, 1n)$, $(\alpha, 2n)$ etc. to distinguish it from the inclusive channel.

To carry out the proof-of-principle experiment, a measurement of the ^{100}Mo(α, xn) cross-section was performed. ^{100}Mo was chosen because the ^{100}Mo$(\alpha, n)^{103}$Ru cross-section has been previously measured via the activation method [13–15]. However, none of the three previous measurements agree within their reported uncertainties. As such, the goal of the present experiment was to measure the ^{100}Mo(α, xn) inclusive cross-section with good enough statistics to resolve the discrepancy between the previous measurements for energies below 10.8 MeV where only the $(\alpha, 1n)$ channel is open.

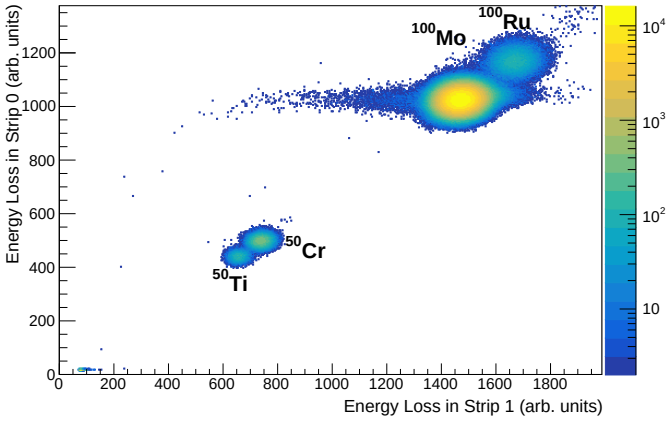

FIG. 1. (Color online) Comparison of the energy losses in the first two strips of MUSIC showing the different components of the beam, at an energy of ∼475 MeV and a gas pressure of 459 Torr. ^{100}Mo is the dominant component and can be easily separated from the contaminants.

II. MEASUREMENT

The experiment was performed in inverse kinematics at the Argonne Tandem Linac Accelerator System (ATLAS) facility using a ^{100}Mo beam. The MUSIC detector was filled with a gas mixture of 95%He and 5%Kr. The purpose of the Kr was to increase the stopping power of the gas mixture so that the relative energy loss difference between Mo and Ru would be larger than the energy resolution of MUSIC while avoiding over-pressurizing the chamber. There were two settings during the experimental run, first a 498.1±0.5 MeV ^{100}Mo beam and a calibrated gas pressure of 408 Torr, followed by a setting with a 474.8±0.5 MeV ^{100}Mo beam and a calibrated gas pressure of 459 Torr. The total beam rate during the experiment was kept under 2000 pps to avoid dead time in the analog data acquisition system. The beam composition is shown in Fig. 1 (E_{beam} = 474.8 MeV, P=459 Torr) and was >98% ^{100}Mo with the largest contaminant being ^{100}Ru (<1%) present in the Mo ion source, as well as ^{50}Ti and ^{50}Cr from previous experiments with Ti. The contaminants were easily separated from the beam by their different energy losses in the first two anode segments of MUSIC, which is strongly dependent on Z. The gas is held in the detector volume by two thin Ti foils (1.35±0.10 mg/cm^2) and secondary reactions may occur since the beam energy is well above the Coulomb barrier. Similar to the beam contaminants, beam-like species which are created by reactions on the Ti foil can be separated from ^{100}Mo.

The experiment measured cross-sections between 8.9 MeV and 13.2 MeV in the center of mass. Within this energy range, both (α, γ) and (α, p) are energetically possible. Simulations show that the separation of (α, p) events from (α, xn) events is challenging with the conditions used in the current experiment, however, the predicted (α, p) cross-sections are 2 orders of magnitude lower than the (α, xn) cross-sections. Thus, any (α, p) events contribute negligibly to the systematic error in the cross-section, far below the statistical errors of the measurement. Without auxiliary neutron detectors, (α, γ) events cannot be distinguished from (α, xn) events, but Hauser-Feshbach calculations (such as from NON-SMOKER) predict that the (α, γ) cross-section to be 3 to 5 orders of magnitude lower than the (α, xn) cross-section. The $(\alpha, 2n)$ channel, which opens at 10.8 MeV, also cannot be distinguished by MUSIC from $(\alpha, 1n)$ events and the inclusive cross-section is measured above 10.8 MeV.

^{100}Mo(α, xn) events are separated from the beam and other α-induced reaction products using a ΔE-DE method (since the beam does not stop in MUSIC). For a given segmented strip, ΔE is calculated as the sum of all the following strips (inclusive of the selected strip) up to the 15th segmented anode strip and DE, the energy deposited in the entire active volume of the detector, is taken from the Frisch grid signal of MUSIC. An additional gate was placed requiring the magnitude of the jump to be above a certain energy loss to eliminate a large number of the α-scattering events. Scattering reactions between ^{100}Mo and Kr would lead to a significant spike in the energy loss and therefore can be easily excluded. Due to the resolution of the anode strip (∼450 keV 1-σ), there is some overlap between (α, xn) events and (α, α) events in the ΔE-DE plot (Fig. 2). Further separation can be achieved through analysis of the energy loss profile across the segmented anode strips, or MUSIC 'traces'.

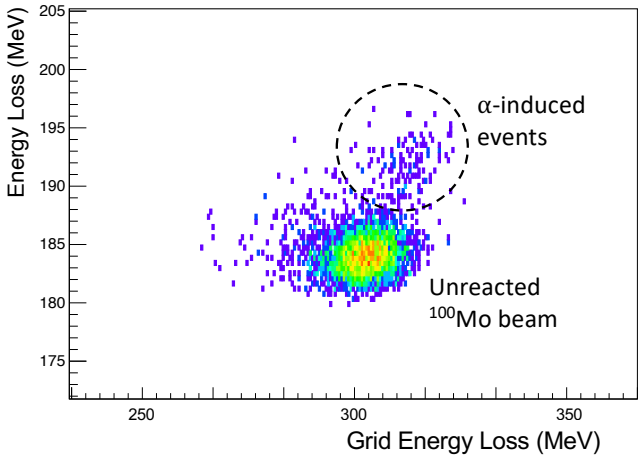

FIG. 2. (Color online:) Energy loss plot of events in the 5th anode strip of MUSIC showing the separation of the different exit channels. The y-axis is the gain-matched summed energy loss over anode strips 5-15 in MeV and the x-axis is the energy loss as measured by the Frisch grid of MUSIC. The approximate analysis gate used for the α-induced events is shown as the dashed oval. The more intense feature is the unreacted ^{100}Mo beam.

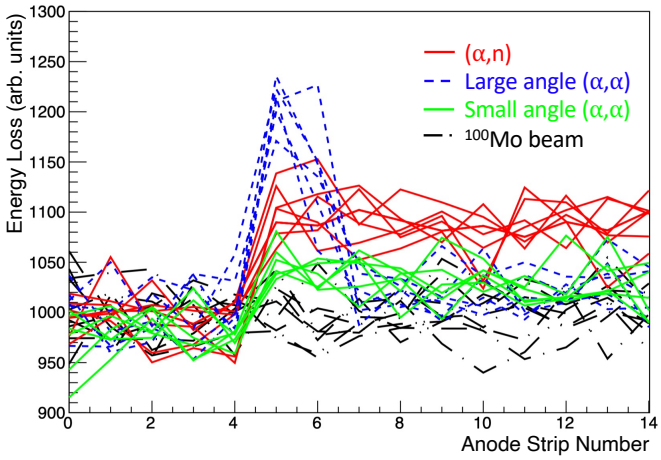

FIG. 3. (Color online:) Energy loss profiles of individual events in MUSIC ('traces'). Traces in black dot-dash are from unreacted Mo beam. (α, xn) events occurring in strip 5 are plotted as solid red lines, showing a characteristic and persistent jump in energy loss that characterizes a change in Z. Large-angle scattering events are shown as blue dashed lines where there is an increase in the energy loss from the scattered α particle over a small number of strips before the energy loss reverts to a beam-like profile. For small-angle scattering events, shown in solid green lines, the scattered α particle travels further along detector, causing a persistent jump in energy loss that is still smaller than that of (α, xn) events.

These traces have been demonstrated in the past to be good identifiers of (α, xn) events, since there is a characteristic 'jump' in the energy loss in the strip where the event happens [11]. In the present energy regime, the energy loss in a segment is proportional to the square of the proton number, Z, as is described by the Bethe formula [16]. In previous MUSIC experiments using lower-Z beams, evaluating the size of this jump is usually sufficient for classification. Due to the small difference in Z between Mo and Ru relative to the proton numbers, the jump is correspondingly smaller with respect to the absolute energy loss in a single strip. This can lead to some ambiguity in classifying certain events at the lowest energies, and we were only able to determine an upper limit for the two lowest energies.

Several experimental traces of unreacted beam, (α, xn), and (α, α) events are shown in Fig. 3. (α, xn) events are characterized by the persistent increase in energy loss implying the creation of the Ru recoil which has two extra protons. Scattering of ^{100}Mo on αs in the detector can mimic (α, xn) events, especially for small scattering angles where the α particles also traverses the length of the MUSIC detector and therefore create a smaller persistent increase in energy loss. For larger scattering angles, the temporary increase in energy loss is larger in magnitude but do no persist because the scattered α particle eventually travels laterally out of the volume of the detector before traversing the detector.

III. RESULTS

The measured angle-integrated cross-sections for center-of-mass energies between 8.9 MeV and 13.2 MeV are shown in Fig. 4 and listed in Tab. I. The center-of-mass energies at each strip were not directly measured but calculated using energy loss tables of ^{100}Mo in the He/Kr gas mixture. Due to the high energy of the beam, the incident ^{100}Mo particles did not stop in MUSIC or lose enough energy to observe the Bragg peak. The center-of-mass energies were calculated with three different energy loss tables from Ziegler [17], ATIMA [18], and eneloss (which uses the original SRIM tables [19]) and show a deviation of up to 7% at the low end of our measured energy range for the measurements at 408 Torr and 6% for the measurements at 459 Torr. The effective energy assigned to each strip was determined from the energy loss at the beginning of the strip (as calculated from the energy loss tables) and corrected for the thick-target yield across the 1.58 cm width of each anode strip. Although this correction depends on the cross-section itself, the uncertainty in the effective energies from the uncertainties in the cross-sections was less than 1% in all cases.

The energies used in Fig. 4 and given in Tab. I are those calculated with ATIMA, as they give the best agreement with the ^{100}Mo$(\alpha, 1n)^{103}$Ru results from [15], spans the energy range covered by an anode strip of MUSIC. The uncertainties of the center-of-mass energies include the contributions from both the choice of energy loss table and the uncertainty in the thickness of the Ti entrance window of MUSIC.

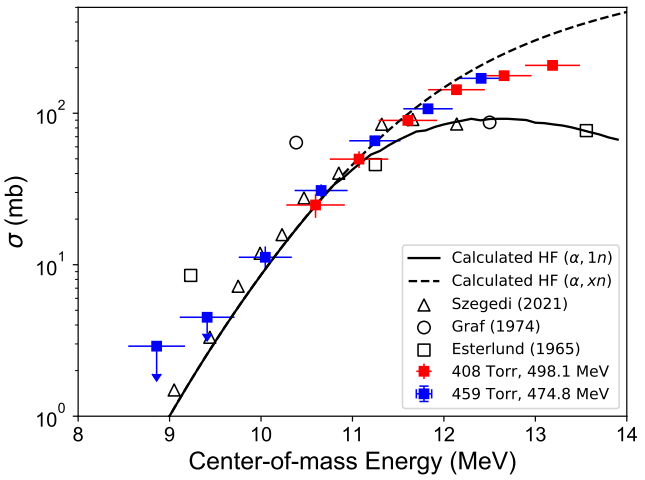

FIG. 4. The measured (α, xn) cross-section in this work at 408 Torr (red squares) and 459 Torr (blue squares), compared with the activation measurements of $(\alpha, 1n)$ from Graf and Münzel [14] (open circles), Esterlund and Pate [13] (open squares), and Szegedi et al. [15] (open triangles). Also shown are the calculated Hauser-Feshbach (α,1n) and total α-induced cross-sections using the ATOMKI-V2 potential, from [15]. Error bars shown here are the statistical errors, and the cross-sections for the two lowest energies measured at 459 Torr are only upper limits.

Our results below the $(\alpha, 2n)$ threshold at 10.8 MeV disagree with both the Graf [14] and Esterlund [13] results. This is puzzling given that one of the conclusions of Graf and Münzel was that the Esterlund results could be reconciled with theirs when more up-to-date (as of 1974) nuclear data was used. A recent activation measurement of the ^{100}Mo$(\alpha, 1n)$ cross-section, performed at ATOMKI [15], also disagrees with the two older measurements.

The new experimental data are compared to calculations from the statistical model in Fig. 4. A detailed discussion of these calculations is given in [15]. Here we only repeat the essential findings of [15]. The calculated total α-induced reaction cross-section depends only on the chosen α-nucleus optical model potential (AOMP). In the energy range under study, the total reaction cross-section is given by the sum over the $(\alpha, 1n)$ and $(\alpha, 2n)$ channels with tiny contributions from the (α, p) and (α, γ) channels of less than 1% which are neglected in the following discussion.

It was found in [15] that Atomki-V2 AOMP [20, 21] provides the best description of the low-energy data in [15]. Other AOMPs like Koning-Delaroche [22] (based on Watanabe [23]), Demetriou *et al.* [24], Avrigeanu *et al.* [25], and McFadden and Satchler [26] show significantly higher or lower cross-sections at low energies below about 10 MeV in the center of mass whereas at higher energies all AOMPs under study in [15] predict quite similar total reaction cross-sections.

Below the $(\alpha, 2n)$ threshold at 10.8 MeV, the new data of the present study agree well with the recent activation data of [15]; both experimental data sets are well described using the Atomki-V2 AOMP. Obviously, above the $(\alpha, 2n)$ threshold the inclusive cross-sections of the present work are higher than the $(\alpha, 1n)$ activation cross-sections of [15] and the earlier data in [13, 14]. Somewhat surprisingly, the new cross-sections at the highest energies under study are lower than the predictions of various AOMPs. This indicates either a deficiency of many AOMPs (which is not very likely) or an underestimation of other channels except (α, xn) in the statistical model.

From the difference between the present inclusive (α, xn) data and the $(\alpha, 1n)$ data from [13–15] we are able to extract the ^{100}Mo$(\alpha, 2n)^{102}$Ru cross-section which is not accessible by activation since ^{102}Ru is stable. We interpolate the calculated $(\alpha, 1n)$ cross-section above 11.6 MeV from [15], shown by the solid black line in Fig. 4 to determine the predicted $(\alpha, 1n)$ cross-sections at the energies measured in this work. Below 11.6 MeV, the calculated $(\alpha, 2n)$ cross-section is consistent with 0. The inferred $(\alpha, 2n)$ cross-sections are given in Table II. The error in the inferred $(\alpha, 2n)$ cross-section is taken to be the sum in quadrature of the error from the MUSIC measurement and the error from the calculated $(\alpha, 1n)$ cross-section from [15]. This error is assumed to be 20%, taken from the factor of 1.2 necessary for agreement between the TALYS calculation and the $(\alpha, 1n)$ cross-section at lower energies.

IV. CONCLUSION

Our measurement has demonstrated that the MUSIC detector can measure inclusive (α, xn) cross-sections on heavy nuclei in inverse kinematics, and is the first measurement of ^{100}Mo(α, xn). Though this is predicated on the assumption that the (α, p) and (α, γ) cross-sections are low at these energies, various Hauser-Feshbach calculations indicate that this is likely to be true for all nuclei that are of interest for the weak r-process [21]. This result, combined with the most recent activation measurement [15], allows the inference of the ^{100}Mo(α,2n)^{102}Ru cross-section. The impact of the new measurement was assessed in weak r-process network calculations, and was not significant in all except the most extreme astrophysical conditions with high entropies, neutron-to-seed and α-to-seed ratios. This is to be expected as high neutron and α densities are needed to overcome the negative Q-values of (α, n) at the Z=50 shell closure so that the nucleosynthetic flow reaches Z=42 for the reaction flow through ^{100}Mo(α, xn) to be important.

This measurement opens the door for future experiments with radioactive beams at facilities such as the Californium Rare Isotope Breeder Upgrade (CARIBU) at ATLAS and the Facility for Rare Isotope Beams (FRIB). In future experiments, there is the possibility to couple MUSIC to neutron detectors such as the Versatile Array of Neutron Detectors at Low Energy (VANDLE) [27] or the Low Energy Neutron Detector Array (LENDA) [28]. The measurement of the neutron multiplicity in coincidence with (α, xn) events, together with the total (α, xn) cross-section, can then be used to determine the individual channels. Such an approach is necessary for (α, n) reactions important to weak r-process nucleosynthesis since, in most cases, the nuclei of interest are unstable and activation is not viable, though such an approach still needs to be tested. With this approach a single measurement with MUSIC could probe both the α optical model potential and γ-strength functions for nuclei far from stability.

This material is based upon work supported by the U.S. Department of Energy, Office of Science, Office of Nuclear Physics, under Contract No. DE-AC02-06CH11357. This research used resources of Argonne National Laboratorys ATLAS facility, which is a Department of Energy Office of Science User Facility. This was work performed under the auspices of the U.S. Department of Energy by Lawrence Livermore National Laboratory under Contract DE-AC52-07NA27344 and with the support of the National Science Foundation under Grant PHY-1430152 (JINA Center for the Evolution of the Elements), NKFIH, Hungary (Gr. No. K134197), US Department of Energy grants DE-FG02-88ER40387 and DE-SC0019042; and US National Nuclear Security Agency through Grant No. DE-NA0003909.

[1] D. Watson, C. J. Hansen, J. Selsing, A. Koch, D. B. Malesani, A. C. Andersen, J. P. Fynbo, A. Arcones, A. Bauswein, S. Covino, *et al.*, Nature **574**, 497 (2019).
[2] F. Montes, T. C. Beers, J. Cowan, T. Elliot, K. Farouqi, R. Gallino, M. Heil, K.-L. Kratz, B. Pfeiffer, M. Pignatari, and H. Schatz, The Astrophysical Journal **671**, 1685 (2007).
[3] S. Woosley and R. D. Hoffman, The Astrophysical Journal **395**, 202 (1992).
[4] Y.-Z. Qian and S. Woosley, The Astrophysical Journal **471**, 331 (1996).
[5] A. Arcones and F. Montes, The Astrophysical Journal **731**, 5 (2011).
[6] L. Hüdepohl, B. Müller, H.-T. Janka, A. Marek, and G. G. Raffelt, Phys. Rev. Lett. **104**, 251101 (2010).
[7] G. Martínez-Pinedo, T. Fischer, and L. Huther, Journal of Physics G: Nuclear and Particle Physics **41**, 044008 (2014).
[8] J. Bliss, A. Arcones, F. Montes, and J. Pereira, Journal of Physics G: Nuclear and Particle Physics **44**, 054003 (2017).
[9] J. Pereira, A. Arcones, J. Bliss, and F. Montes, Journal of Physics: Conference Series **1668**, 012033 (2020).
[10] P. F. F. Carnelli, S. Almaraz-Calderon, K. Rehm, M. Albers, M. Alcorta, P. Bertone, B. Digiovine, H. Esbensen, J. F. Niello, D. Henderson, *et al.*, Nuclear Instruments and Methods in Physics Research Section A: Accelerators, Spectrometers, Detectors and Associated Equipment **799**, 197 (2015).
[11] M. L. Avila, K. E. Rehm, S. Almaraz-Calderon, A. D. Ayangeakaa, C. Dickerson, C. R. Hoffman, C. L. Jiang, B. P. Kay, J. Lai, O. Nusair, R. C. Pardo, D. Santiago-Gonzalez, R. Talwar, and C. Ugalde, Phys. Rev. C **94**, 065804 (2016).
[12] R. Talwar, M. Bojazi, P. Mohr, K. Auranen, M. Avila, A. Ayangeakaa, J. Harker, C. Hoffman, C. Jiang, S. Kuvin, *et al.*, Physical Review C **97**, 055801 (2018).
[13] R. Esterlund and B. Pate, Nuclear Physics **69**, 401 (1965).
[14] H. Graf and H. Muenzel, Journal of Inorganic and Nuclear Chemistry **36**, 3647 (1974).
[15] T. N. Szegedi, G. G. Kiss, P. Mohr, A. Psaltis, M. Jacobi, G. G. Barnaföldi, T. Szücs, G. Gyürky, and A. Arcones, Phys. Rev. C **104**, 035804 (2021).
[16] H. A. Bethe and J. Ashkin, Wiley, New York (1953).
[17] J. F. Ziegler, M. D. Ziegler, and J. P. Biersack, Nuclear Instruments and Methods in Physics Research Section B: Beam Interactions with Materials and Atoms **268**, 1818 (2010).
[18] H. Weick, H. Geissel, N. Iwasa, C. Scheidenberger, and J. R. Sanchez, GSI Scientific Report (2017).
[19] J. F. Ziegler and J. P. Biersack, in *Treatise on heavy-ion science* (Springer, 1985) pp. 93–129.
[20] P. Mohr, Z. Fülöp, G. Gyürky, G. G. Kiss, and T. Szücs, Phys. Rev. Lett. **124**, 252701 (2020).
[21] P. Mohr, Z. Fülöp, G. Gyürky, G. Kiss, T. Szücs, A. Arcones, M. Jacobi, and A. Psaltis, Atomic Data and Nuclear Data Tables **142**, 101453 (2021).
[22] A. Koning and J. Delaroche, Nuclear Physics A **713**, 231 (2003).
[23] S. Watanabe, Nuclear Physics **8**, 484 (1958).
[24] P. Demetriou, C. Grama, and S. Goriely, Nuclear Physics A **707**, 253 (2002).
[25] V. Avrigeanu, P. E. Hodgson, and M. Avrigeanu, Phys. Rev. C **49**, 2136 (1994).
[26] L. McFadden and G. Satchler, Nuclear Physics **84**, 177 (1966).
[27] W. Peters, S. Ilyushkin, M. Madurga, C. Matei, S. Paulauskas, R. Grzywacz, D. Bardayan, C. Brune, J. Allen, J. Allen, Z. Bergstrom, J. Blackmon, N. Brewer, J. Cizewski, P. Copp, M. Howard, R. Ikeyama, R. Kozub, B. Manning, T. Massey, M. Matos, E. Merino, P. O'Malley, F. Raiola, C. Reingold, F. Sarazin, I. Spassova, S. Taylor, and D. Walter, Nuclear Instruments and Methods in Physics Research Section A: Accelerators, Spectrometers, Detectors and Associated Equipment **836**, 122 (2016).
[28] G. Perdikakis, M. Sasano, S. M. Austin, D. Bazin, C. Caesar, S. Cannon, J. Deaven, H. Doster, C. Guess, G. Hitt, J. Marks, R. Meharchand, D. Nguyen, D. Peterman, A. Prinke, M. Scott, Y. Shimbara, K. Thorne, L. Valdez, and R. Zegers, Nuclear Instruments and

Methods in Physics Research Section A: Accelerators, Spectrometers, Detectors and Associated Equipment **686**, 117 (2012).

TABLE I. Cross-sections measured in this work. The center-of-mass energies and energy ranges given were calculated using the ATIMA 1.4 energy loss tables and are corrected for the thick-target yield across each strip of the MUSIC detector. The error given in the effective energies arises mainly due to systematic differences between the different energy loss tables. The errors given for the cross-sections (mb) are predominantly statistical and the asterisks indicate upper limits on the cross-sections for the two lowest energy points.

	P = 459 Torr			P = 408 Torr	
$E_{cm,eff}$ (MeV)	E range (MeV) [a]	σ (mb)	$E_{cm,eff}$ (MeV)	E range (MeV) [a]	σ (mb)
12.43 (0.26)	12.68 - 12.10	170 (10)	13.17 (0.30)	13.44 - 12.91	196 (12)
11.84 (0.27)	12.10 - 11.50	107 (7)	12.65 (0.30)	12.91 - 12.38	172 (11)
11.25 (0.28)	11.50 - 10.90	66 (5)	12.14 (0.31)	12.38 - 11.84	140 (10)
10.66 (0.29)	10.90 - 10.29	31 (3)	11.59 (0.32)	11.84 - 11.30	71 (7)
10.05 (0.29)	10.29 - 9.69	11 (2)	11.06 (0.32)	11.30 - 10.76	43 (5)
9.41 (0.30)	9.69 - 9.10	4.5 [b]	10.59 (0.32)	10.76 - 10.21	22 (4)
8.86 (0.31)	9.10 - 8.49	2.9 [b]			

[a] ATIMA 1.4
[b] upper limit

TABLE II. Inferred ^{100}Mo$(\alpha, 2n)^{102}$Ru cross-sections using the results from this work and the calculated Hauser-Feshbach rate with the Atomki-V2 α optical model potential from [15]. See text for the details of the reported unncertainties.

Energy (MeV)	$(\alpha, 2n)$ cross-section (mb)
11.84	27 (17)
12.14	52 (20)
12.43	79 (21)
12.65	80 (21)
13.17	111 (21)